Dynamic Albedo of Neutrons (DAN) experiment onboard NASA's Mars Science Laboratory

Article *in* Space Science Reviews · September 2012

DOI: 10.1007/s11214-012-9924-y

CITATIONS
33

READS
189

23 authors, including:

A. Behar
NASA
91 PUBLICATIONS **1,708** CITATIONS
SEE PROFILE

William V. Boynton
The University of Arizona
791 PUBLICATIONS **10,935** CITATIONS
SEE PROFILE

Shvetsov Valery
Joint Institute for Nuclear Research
125 PUBLICATIONS **917** CITATIONS
SEE PROFILE

Gennady Nikolaevich Timoshenko
Joint Institute for Nuclear Research
75 PUBLICATIONS **231** CITATIONS
SEE PROFILE

Space Sci Rev (2012) 170:559–582
DOI 10.1007/s11214-012-9924-y

Dynamic Albedo of Neutrons (DAN) Experiment Onboard NASA's Mars Science Laboratory

I.G. Mitrofanov · M.L. Litvak · A.B. Varenikov · Y.N. Barmakov · A. Behar · Y.I. Bobrovnitsky · E.P. Bogolubov · W.V. Boynton · K. Harshman · E. Kan · A.S. Kozyrev · R.O. Kuzmin · A.V. Malakhov · M.I. Mokrousov · S.N. Ponomareva · V.I. Ryzhkov · A.B. Sanin · G.A. Smirnov · V.N. Shvetsov · G.N. Timoshenko · T.M. Tomilina · V.I. Tret'yakov · A.A. Vostrukhin

Received: 19 January 2012 / Accepted: 13 July 2012 / Published online: 28 July 2012

Abstract The description of Dynamic Albedo of Neutrons (DAN) experiment is presented, as a part of the NASA's Mars Science Laboratory mission onboard the mars rover Curiosity. The instrument DAN includes Pulsing Neutron Generator (PNG) producing pulses of 14.1 MeV neutrons for irradiation of subsurface material below the rover, and Detectors and Electronics (DE) unit, which operates the instrument itself and measures the die-away time profiles of epithermal and thermal neutrons following each neutron pulse. It is shown that the DAN investigation will measure a content of hydrogen along the path of the MSL rover, and it will also provide information about a depth distribution of hydrogen at 10–20 regions selected for the detailed studies and sampling analysis.

Keywords Mars exploration · Detection of water · Active neutron experiment

I.G. Mitrofanov (✉) · M.L. Litvak · A.B. Varenikov · A.S. Kozyrev · R.O. Kuzmin · A.V. Malakhov · M.I. Mokrousov · A.B. Sanin · V.I. Tret'yakov · A.A. Vostrukhin
Space Research Institute, Profsouznaya street 84/32, Moscow, 117997, Russia
e-mail: imitrofa@space.ru

Y.N. Barmakov · E.P. Bogolubov · V.I. Ryzhkov · G.A. Smirnov
All-Russian Institute of Automatics, Moscow, 101000, P.O. Box 918, Russia

A. Behar · E. Kan
Jet Propulsion Laboratory, California Institute of Technology, 4800 Oak Grove Drive, Pasadena, CA 91109, USA

Y.I. Bobrovnitsky · S.N. Ponomareva · T.M. Tomilina
A.A. Blagonravov Institute of Mechanical Engineering, M. Hariton'evskii per., 4, Moscow, 101990, Russia

W.V. Boynton · K. Harshman
Lunar and Planetary Laboratory, University of Arizona, Tucson, USA

V.N. Shvetsov · G.N. Timoshenko
Joint Institute of Nuclear Research, Dubna, Russia

List of Abbreviations

ASA	Active Surface Analysis
ASM	Active Surface Monitoring
CEN	Counter of Epithermal Neutrons
CTEN	Counter of Thermal and Epithermal Neutrons
DAN	Dynamic Albedo of neutrons
DE	Detectors and Electronics
FWHM	Full Width Half Maximum
GCR	Galactic Cosmic Rays
HCAS	Hydrogen or Chemical Anomaly Spot
ING	Industrial Neutron Generator
MCNPX	Monte Carlo Neutrons Protons X-rays
MeV	Mega electron Volt
MMTRG	Multi Mission Radioisotope Thermoelectric Generator
MSL	Mars Science Laboratory
PDS	Planetary Data System
PNG	Pulsing Neutron Generator
PSA	Passive Surface Analysis
SPE	Solar Particle Event

1 Introduction

One of the main goals of NASA's Mars Science Laboratory is to test whether Mars ever has, or still has today, an environment for supporting microbial life and conditions for planet habitability (see Grotzinger et al. 2012, this issue). Also, the history of Mars' hydrological evolution and sedimentation is another equally important goal for investigations on MSL. It is commonly accepted that reconnaissance of water rich spots, spots with unusually high hydration of minerals of the soil, or spots with some chemical anomalies would be a necessary condition for the accomplishment of these goals. Indeed, if a *Hydrogen or Chemical Anomaly Spot* (HCAS) would be identified, the package of MSL analytical instruments could perform the comprehensive studies of soil composition in the shallow subsurface for determining the history of sedimentation and looking for biomarkers. The MSL landing site at the crater Gale should have many such spots, but the uppermost layer of the crater surface could be a blanket of dust, which is the same everywhere. To find the best HCAS for detailed analysis, MSL needs a tool for remote sensing of the shallow subsurface along the rover path, that allows it to detect the enhancement of hydrated minerals, or absorbed water (even water ice), or anomalies of chemical composition under the dusty top layer on the surface. This tool is the active neutron instrument DAN (*Dynamic Albedo of Neutrons*), which is contributed to NASA's MSL mission for the joint investigation of Mars by the Federal Space Agency of Russia.

In this paper we describe the physics of the DAN investigation (Sect. 2), present details on the instrument design (Sect. 3) and discuss the capabilities to detect hydrogen enhanced and/or chemical anomaly spots on the Martian surface (Sect. 4). We have also considered the possible strategy of DAN measurements onboard MSL (Sect. 5). Section 6 concludes with the main expected results of DAN investigation.

2 Physics of DAN Investigation

2.1 Origin of Neutrons at the Top Layer of a Planetary Body

It has been known for a long time that planetary bodies without or with thin atmospheres produce the proper emission of neutrons and gamma-rays from the shallow subsurface due to bombardment by energetic particles of *Galactic Cosmic Rays* (GCR) and *Solar Particle Events* (SPE), see for example Arnold et al. (1962), Drake et al. (1988). There are a number successfully accomplished space experiments for measurements of this emission, which allowed collection of essential observational data about the chemical composition of tested planetary bodies. It has been accomplished for the Moon by Luna-10 (Vinogradov et al. 1966), by Apollo 15 and 16 (Metzger et al. 1973), by Lunar Prospector (Feldman et al. 2004a) and by Lunar Exploration Neutron Detector (Mitrofanov et al. 2008, 2010a). For small bodies like the asteroid Eros and Vesta it was measured by NEAR (Evans et al. 2001) and DAWN (Prettyman et al. 2011) missions. Mars was studied by Phobos-2 (d'Uston et al. 1989) and by Mars Odyssey (Boynton et al. 2002, 2004) missions. Finally, mapping of Mercury surface has being started by MESSENGER (Goldsten et al. 2007; Rhodes et al. 2011). In particular, the orbital remote sensing measurements of neutrons allowed mapping deposits of water ice on Mars and at the Moon (see Boynton et al. 2002; Mitrofanov et al. 2002, 2003, 2004, 2010b; Feldman et al. 2001, 2002, 2004b; Litvak et al. 2006; Prettyman et al. 2004).

A more sophisticated method for landed missions was suggested by Adler and Trombka (1970) based on the active irradiation of a planetary surface with pulses of high energy neutrons (produced by a *Pulsing Neutron Generator* (PNG)) and measuring its neutron albedo and induced gamma rays (similar to Earth geological applications). Instruments using such an approach have not been flown in space, but the method itself and related instrumentation has been discussed many times (e.g. see Akkurt et al. 2005; Jun et al. 2011; Parsons et al. 2011). DAN is the first implementation of such an instrument with a pulse neutron generator developed for space exploration (onboard the MSL mission), which would provide new opportunities for studies of the martian surface *in situ*, as shown below (see also Litvak et al. 2008).

2.2 Neutrons Diffusion and Moderation Processes at the Surface of a Planetary Body

The physics of both passive and active neutron experiments for sensing of a planetary body is associated with interactions between atomic nuclei in the soil and neutrons, which are either produced naturally by GCRs, or generated artificially by a PNG. The neutrons have originally the high energy E_0 about 10–20 MeV or 14.1 MeV for these two cases, respectively. They are either produced naturally in nuclear spallation reactions by energetic particles of GCR and SPE, or injected artificially by a PNG into the surface. The depth of neutron propagation L is about 1 meter, which is much larger than a mean free path l_{fp} between interactions with nuclei of a soil. Therefore, neutrons leak out from the surface by the process of diffusion, which is accompanied by their moderation down to thermal energies due to elastic collisions with nuclei, and also by emission of secondary gamma-rays due to non-elastic collisions with nuclei. The average number N_{leak} of random walks of a neutron for leakage from the depth L is proportional to $(L/l_{fp})^2 \gg 1$.

An energetic neutron with energy E loses its energy at each collision. The maximum of lost energy corresponds to a head-on collision of an incoming neutron, when a target nucleus recoils in the same direction

$$\delta E_{max} = 4A(1+A)^{-2}E, \tag{1}$$

where A is the atomic mass of a nucleus (Knoll 2000). Such decrease in energy of energetic neutrons during diffusion is referenced as a *moderation* process, which is a "cooling" of neutrons in the environment of thermal nuclei. The final state of moderation is a *thermalization* of neutrons. It corresponds to the thermal equilibrium between neutrons and nuclei of a soil. For a given composition of a soil, one may estimate the number of collisions N_{th} for thermalization.

Some neutrons may leak from the subsurface during random walks, and this leakage could occur either at the intermediate stage of moderation, or after thermalization. Other neutrons are absorbed by nuclei in capture reactions or decay deep in the subsurface—we do not consider these particles below.

So, one may say that neutrons leaked from the surface of a planetary body have diffused in the volume of 5-parameter space before the leakage. Three dimensions of this volume are spatial coordinates in the subsurface. The fourth dimension is the neutron kinetic energy E, which may change in each collision. The leaking neutron has an energy range from E_{th} to E_0. The fifth dimension represents time intervals between successive collisions. Each leaking neutron can be attributed with time parameter t corresponding to the total leakage time measured from the initial moment t_0 of neutron production or injection to the moment of its escaping. The sample of leaking neutrons may be characterized by the average leakage time t_{leak}. The leaking neutrons with larger leakage time have smaller energy, and vice versa.

The evolution of the energy spectrum of leaking neutrons after pulses has been calculated by Monte Carlo numerical simulations (Fig. 1). In a short time after pulses (several μs) the spectrum has a high energy peak around the energy of production E_0. In long time after pulses (several milliseconds) the spectrum has the low energy peak around E_{th}, which corresponds to thermal equilibrium. The intermediate part of the spectrum corresponds to epithermal neutrons escaped from the subsurface before thermalization. The amplitude of the thermal component and shape of the intermediate part of epithermal neutrons depend on the ratio between leakage time t_{leak} and thermalization time t_{th}. If thermalization process takes more time than the leakage ($t_{leak} < t_{th}$), then the majority of particles may escape from the surface before thermalization (see Fig. 1). This case takes place if the soil consists of heavy nuclei, and as a result neutrons lose rather small energy $\delta E_{max} \ll E$ at each individual elastic collision (see Eq. (1)). The energy spectrum has a small thermal peak and a high intermediate component of epithermal neutrons in this case (Fig. 1). The presence even of a small fraction of hydrogen in the soil significantly increases the efficiency of moderation. In this case an energy loss at the single elastic collision of neutron with hydrogen nuclei (proton) may be comparable with the initial energy: $\delta E_{max} \sim E$ (see Exp. (1)). So higher content of hydrogen leads to the decreasing of number of collisions required for thermalization N_{th}.

In hydrogen rich soil N_{th} becomes smaller in comparison with N_{leak}. The thermal component dominates the spectrum of leaking neutrons in this case, while the epithermal component of the spectrum is significantly suppressed. Also, one has to take into account that faster thermalization leads to a decrease in the average velocity of neutrons during random walks. Leaking neutrons with the same number of random walks will thus need a longer time to leak if they were quickly thermalized at the initial stage of diffusion. Numerical simulations of DAN investigations have shown that these two complementary effects, increase of thermal component and delay of die-away emission, are easily visible for soils with increasing content of hydrogen.

Together with moderation, a process of random walks of neutrons is accompanied by their absorption in the nuclear capture reactions. Thus, the nuclei of hydrogen might capture a neutron with the production of deuterium and emission of a photon with energy 2.2 MeV. Several nuclei abundant in the subsurface of planetary bodies (like Cl and Fe, see for example Lawrence et al. 2002; Diez et al. 2009) have rather large cross sections for neutron

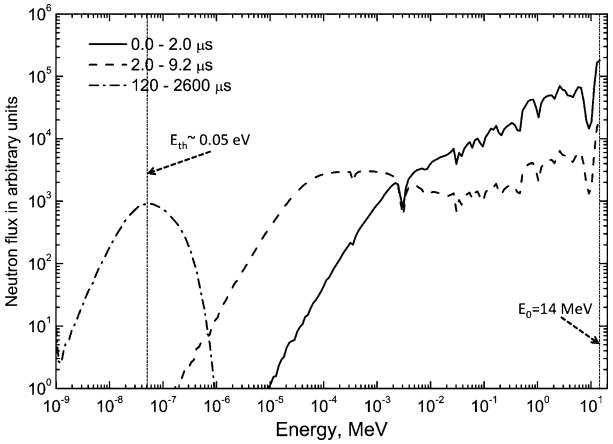

Fig. 1 The calculated energy spectra of neutrons from the Martian subsurface irradiated by the pulse of $E_0 = 14$ MeV (shown on the plot by *dotted vertical line*) neutrons from DAN PNG. The *solid black curve* corresponds to the energy spectrum of neutrons within time window 0–2 microseconds after the neutron pulse, *dashed curve* corresponds to the time window 2–10 microseconds and *dash-dotted curve* corresponds to the time window 120–2600 microseconds. The energy $E_{th} \sim 0.05$ eV corresponding to the peak of thermal neutrons is also shown on the plot as *dotted vertical line*

absorption, which increases with decreasing neutron energy. Neutron absorption has a significant effect on the neutron distribution in the subsurface and should be taken into account in the interpretation of the neutron leakage process.

2.3 Why Measurements of the Dynamic Albedo of Neutrons Are Necessary for MSL

The proper emission of neutrons produced by GCRs in the Moon, Mars and Mercury subsurface has been successfully measured with very high science output. The analysis of neutron data from Mars and Moon has provided the knowledge about the global distribution of hydrogen and high absorbing elements in the subsurface of these planetary bodies (see introduction section for reference details). Currently the gamma and neutron data are being produced by MESSENGER'S neutron spectrometer for Mercury (see Rhodes et al. 2011; Riner et al. 2011). Generally speaking, one could suggest that measurements of thermal and epithermal neutrons due to GCRs could be enough for testing hydrogen variations along the traverse of the MSL rover. Moreover, MSL is supplied with the Multi Mission Radioisotope Thermoelectric Generator (MMRTG), which produces a flux of neutrons in a wide energy range (from thermal up to fast neutrons) due to the decay of ^{238}Pu. These MMRTG neutrons also participate in the diffusion and moderation process in the subsurface.

Therefore, the passive neutron measurements onboard MSL would characterize the *static albedo of neutrons* from two different sources: the nuclear cascades in the subsurface due to GCRs, and irradiation by the MMRTG. Neutrons from these two sources have different initial energies and different depth distributions, so one should include both sources of neutrons into the single model for the diffusion-and-moderation process for interpreting the observed energy spectrum of leaking neutrons.

However, such measurements of the static neutron albedo could not properly match the main goals of MSL, even if all details of diffusive leakage of neutrons from GCR and from the MMRTG were properly taken into account. The accomplishment of the MSL goals requires a characterization of depth distribution of hydrogen in the Martian soil along the trace

of the rover. It is necessary for the scientific analysis of layering structure of the hydrogen bearing minerals. This information also will be requested for planning rover operations related with sampling hydrogen bearing minerals from the subsurface.

One of the ways to provide a detailed study of the hydrogen depth distribution is based on measuring of the distribution of intervals of neutron leakage time between moments of origin and escaping. This distribution is not available in the observations of static neutron albedo because one cannot determine when an individual neutron started its diffusion. During the motion of the rover, passive detectors will measure spatial variations of thermal and epithermal neutrons induced by CGRs and MMRTG, which helps to estimate changes of bulk composition of subsurface hydrogen rich material and derive some rough indications how it could be distributed as a function of depth. But to resolve depth structure of hydrogen bearing layers in the subsurface with more additional details, one has to measure the *dynamic albedo of neutrons* (the designation of this process was selected to name the instrument DAN described in the paper). Generally speaking, it means that one needs to fix a moment t_0, when all neutrons with high energy E_0 are instantaneously inserted into the subsurface, and then to measure the energy and leakage time intervals t_{leak} of the leaking neutrons. In other words, one needs to measure the time evolution of the spectrum of leaking neutrons in respect to the moment of neutron origin in the subsurface.

The average leakage time values t_{leak} of epithermal and thermal neutrons range from tens of microseconds up to several milliseconds. The corresponding neutron fluxes also may vary by several times, representing the content of hydrogen and indicating the presence of chemical anomalies in the subsurface. One may conclude that DAN time-dependent measurements of thermal and epithermal energy ranges allow the detection of *Hydrogen and Chemical Anomaly Spots* (HCASs) with high content of hydrogen and neutron absorbing elements and provide the information about their depth distribution in the subsurface.

2.4 Physical Measurements of DAN Investigation

DAN is an active experiment on the surface of Mars, that irradiates the soil by pulses of 14.1 MeV neutrons. The instrument measures two die-away time profiles of epithermal and thermal neutrons after each pulse injection (Fig. 2). These time profiles present distributions of leakage time intervals for epithermal and thermal neutrons, which have been moderated or thermalized, respectively. There is a clear distinction in the neutron arrival time at the detector volume between the shorter times of epithermal neutrons and much longer times for thermal neutrons.

As explained above, the moderation of high energy neutrons is quicker in a soil with a higher hydrogen content. Comparing die-away time profiles of epithermal and thermal neutrons for the soil with lower and higher content of hydrogen, one sees that emission of the thermal component is much longer and larger for higher hydrogen abundance, and, correspondingly, the epithermal component is faster and smaller (Fig. 2). However, one needs to take into account that for increasing content of hydrogen there is no exact conservation of moderating particles at the sum of the epithermal and thermal domains: Hydrogen nuclei not only moderate but also absorb neutrons, preferably thermal neutrons with low energy. Nevertheless the inter-relation between the emission of thermal and epithermal neutrons works well to produce the signature of variations in the bulk content of hydrogen in the soil.

Die-away profiles of neutrons have different shapes for soils with different depth distributions of hydrogen. Indeed, let us consider the simplest case when a sample of neutrons leaks from the same depth L with the same number of collisions N_{fp}. The time of leaking may be estimated as $t_{leak} = N_{fp} \cdot l_{fp}/V_{av}$, where V_{av} is the average velocity of neutrons during diffusion. If a hydrogen bearing soil is at the top just below the

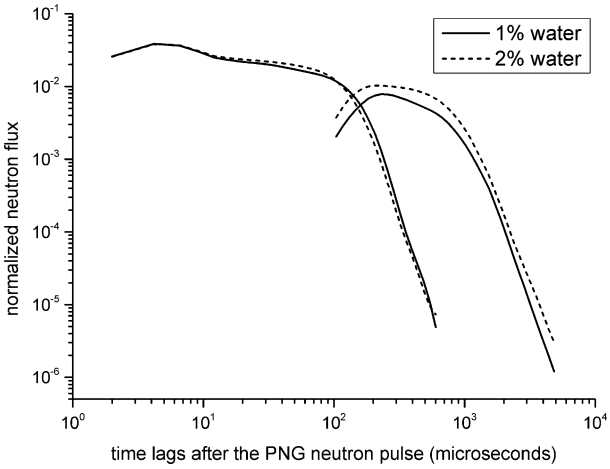

Fig. 2 The numerically simulated die-away curves of epithermal (*left part of the figure*) and thermal (*right part of the figure*) neutrons produced in the Martian subsurface with different content of water: 1 % (*solid line*) and 2 % (*dashed line*). It is seen that the signature of water increase is more pronounced for the thermal component of die-away emission

surface, leaking neutrons are thermalized at the final stage of diffusion, and the time for leaking $t_{leak}^{(H\ top)}$ is determined by V_{av}, which is $\gg V_{th}$. If the same soil lies at the depth L, neutrons are thermalized at the beginning of diffusion, and $V_{av} \sim V_{th}$. Therefore, one gets $t_{leak}^{(H\ depth)} \gg t_{leak}^{(H\ top)}$. In the real case one needs to perform Monte Carlo simulations to relate the profile of die-away emission of neutrons with the layering structure of the hydrogen-bearing soil. There were several numerical simulations of DAN measurements published for different subsurface layering (see Busch and Aharonson 2009; Litvak et al. 2008) as well as several experimental measurements for different layering structure of the soil (Litvak et al. 2010, 2011). Both the numerical analysis and the field measurements proved that DAN is capable of measuring the layering structure of hydrogen H deposition in the upper subsurface (see Sect. 4 below), as required to address the objectives of the MSL mission.

It is also important to consider the effects of varying abundances of high absorption elements Cl and Fe, which are likely to be found on the Martian surface. The first attempt of joint modeling of H and Cl compositions has been done by Hardgrove et al. (2011). They demonstrated that both elements will significantly affect DAN's thermal neutron count rates. Additionally they have shown that timing analysis of die-away curves may independently determine the abundances of hydrogen and high neutron absorption elements (primarily Cl).

3 DAN Instrumentation

3.1 The Design Concept of DAN

The instrument DAN (Dynamic Albedo of Neutrons) is the first instrument in space that applies the active methods of nuclear science for studying another planetary body. High energy neutrons at 14.1 MeV are produced by *Pulsing Neutron Generator* (PNG) in short pulses with duration of about 2–3 microseconds. DAN/PNG has a vacuum tube with an electrostatic accelerator of $^2H^+$ ions to provide their collisions with the nuclear target enriched with ^3H. Alternative possibilities in the selection a neutron generator for DAN were also studied at the instrument development stage. We considered the models of neutron generators supplied with gas-filled tubes instead of vacuum ones. Finally the option with gas-filled

Table 1 DAN/PNG (flight unit) parameters

Parameter	Value
Max Dimensions	$125 \times 45 \times 338$ mm
Mass	2.6 kg
Energy of emitted neutrons	14.1 MeV
Number neutron per pulse	1.34×10^7
Total number pulses can be emitted per life time	$>10^7$
Duration of neutron pulse (FWHM)	<2 microseconds
Frequency of pulsing	From single pulses up to 10 Hz
Power in duty mode (power on)	0.1 W
Power in enabling mode (ready to pulse)	1.4 W
Power in pulsing mode	13 W
Operation temperature range	[−40, +50] °C
Survival temperatures	[−55, +75] °C
Input Voltage range (Normal operations)	22–36 V
Input Voltage range (Surviving)	0–40 V
Readiness to operate after switching power on	<2 sec
Warranty (life time of neutron tube)	3 years or 10^7 pulses

tubes was rejected because such neutron generators produce rather long pulses of neutron emission with duration about several tens of microseconds. Using such a generator, it is impossible to measure the earliest phase of die-away of neutron dynamic albedo when neutrons are first leaking from the surface. The PNG with the vacuum tube provided the possibility to start measurements of neutron albedo within several microseconds after a pulse (see instrument specifications in the Tables 1 and 2). In the DAN instrument, the die-away profiles for thermal and epithermal neutrons are detected individually after each pulse. They are measured with high statistical confidence, as a sum of counts within a set of time window lags after each neutron pulse, and they are averaged for many pulses.

The active neutron method of detection of hydrogen bearing materials is being used for various geological applications. The best known one is the neutron logging technique where a neutron source (pulse neutron generator) along with neutron and gamma detectors are lowered into the well for monitoring the presence of hydrocarbons in the material around the well (see for example overview edited by Ellis and Singer 2007). The design of the flight model of DAN/PNG is based on the heritage of the industrial prototype, ING-101, which has been developed by the N.L. Dukhov Institute of Automatics (Moscow, Russia) and successfully used for many years in numerous geological applications.

The instrument DAN has two separate units: *Pulsing Neutron Generator* (DAN/PNG) (Fig. 3) and the block of *Detectors and Electronics* (DAN/DE) (Fig. 4), which are installed at the two back corners of the MSL rover (Fig. 5). DAN/DE is connected to the subsystems of the rover, and it performs all logical-operational and data telemetry functions of the instrument together with neutron detection and signal processing.

3.2 DAN/PNG Unit

The DAN/PNG, with a mass of 2.6 kg (Fig. 3, Table 2) is actually a miniature nuclear fusion reactor, which produces α-particles with an energy of 3.5 MeV and neutrons with

Table 2 DAN/DE (flight unit) parameters

Parameter	Value
Max Dimensions	204 × 61 × 212 mm
Mass	2.10 kg
Number of detectors	2 (CTEN and CEN)
Neutron energy (detected neutrons)	<1 keV (CTEN detector) 0.4 eV–1 keV (CEN detector)
Number of spectra channels per each detector	16 (linear)
Time scale per each detector	64 (logarithmic)
Duration of lowest time bin	2 microseconds
Spatial resolution	<1 m
Power in passive mode	3.7 W (22 V)–4.5 W (36 V)
Power at standby mode	2.8 W (22 V)–3.5 W (36 V)
Warranty	5 years
Operation temperature range	[−40, +50] °C
Survival temperatures	[−55, +70] °C
Input Voltage range (Normal operations)	22–36 V
Input Voltage range (Surviving)	0–40 V
Readiness to operate after switching power on	<1 sec
Warranty (life time of neutron tube)	3 years

Fig. 3 Photo of Flight unit of DAN/PNG

an energy of 14.1 MeV in the classical nuclear fusion reaction of hydrogen isotopes $^2\mathrm{H} + {}^3\mathrm{H} \rightarrow {}^4\mathrm{He} + \mathrm{n}$. This reaction requires an energy threshold and takes place if the relative kinetic energy of deuterium and tritium is about 100 keV to overcome the Coulomb barrier. The reaction occurs inside the vacuum tube of the PNG, which is a small electrostatic accelerator of deuterium ions produced by the ion source with an electrical potential of 120 kV. This tube is the main component of the DAN/PNG.

The DAN/PNG produces about 10^7 neutrons per pulse with pulse duration of 2–3 microseconds. The pulsing frequency varies from a single pulse mode up to 10 Hz. The vacuum tube is designed to provide up to 10^7 pulses during the lifetime of DAN/PNG. It means that DAN has a limited capability for pulsing, which should be taken into account in the strategy of DAN operations. The 14.1 MeV neutrons diffuse within 1 meter layer of the shallow subsurface, and a portion of them leak out as the dynamic albedo emission as a function of time after the neutron pulse. The emission of neutron die-away profiles becomes negligible after tens of milliseconds, which is $\sim 10^4$ times longer than the DAN/PNG pulse duration, and at least several times less than the shortest period between pulsing (100 milliseconds at 10 Hz of pulsing). Therefore, the DAN/PNG provides adequate capabilities to measure time-

Fig. 4 Photo of Flight unit of DAN/DE

resolved dynamic albedo of epithermal and thermal neutrons induced by pulses of 14.1 MeV neutrons.

3.3 DAN/DE Unit

DAN/DE with mass of 2.1 kg (Fig. 4) has two standard gas proportional counters filled with ^{3}He, under the pressure of 3 atmospheres. It uses a well-known technique used in nuclear science to measure fluxes of thermal and epithermal neutrons. The detection reaction is a capture of a neutron by the nuclei of ^{3}He ($n + {}^3He \rightarrow p + T$) accompanied by the production of a proton and a triton per each detected neutron. The total energy released in this reaction is distributed in the proportion of 573 keV for the proton and 191 keV for the triton. The cross-section of this reaction increases with decreasing neutron energy, so ^{3}He counters are mainly used for detection of thermal and low energy epithermal neutrons. The counters have a diameter of 5.1 cm and a length of 6.5 cm with a ~4 cm active zone (manufactured by LND Ltd, type 253146). One counter is used as a *Counter of Epithermal Neutrons* (CEN). It is covered by an enclosure of 1-mm thick cadmium, which is a strong absorber of neutrons below the energy ~0.4 eV. We will therefore use this value, as the conventional boundary of thermal and epithermal neutrons (see Fig. 6). Another counter is covered by a lead enclosure with thickness of 1 mm, and works as the *Counter of Thermal and Epithermal Neutrons* (CTEN). Lead does not absorb neutrons, but absorb X-rays, which are produced by PNG during a pulse (the *Cd* enclosure of CEN absorbs these X-rays as well as lead of CTEN).

For both CEN and CTEN sensors, the neutron counts are detected as 16 energy-channel spectra. For each counter, the detection reaction has the same spectrum of counts, which represents the energy deposition from the detection reaction in the volume of the sensor. The measurement of these spectra during preflight calibrations allows one to distinguish, if necessary, counts from neutrons and counts from background of gamma-rays and charged particles, or from electronic noise.

For measuring die-away time profiles of the dynamic albedo of neutrons, DAN/DE performs the measurement of time lags for each neutron count (detected in CEN and CTEN), as

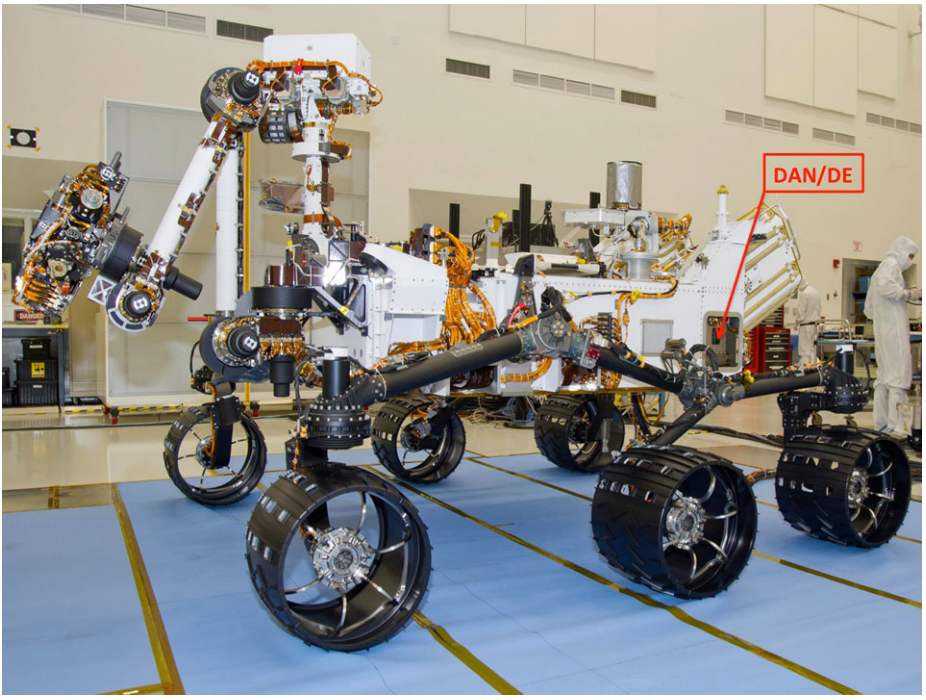

Fig. 5 Photo of accommodation of DAN (DAN/DE) onboard of MSL rover (courtesy of http://mars.jpl.nasa.gov/msl/)

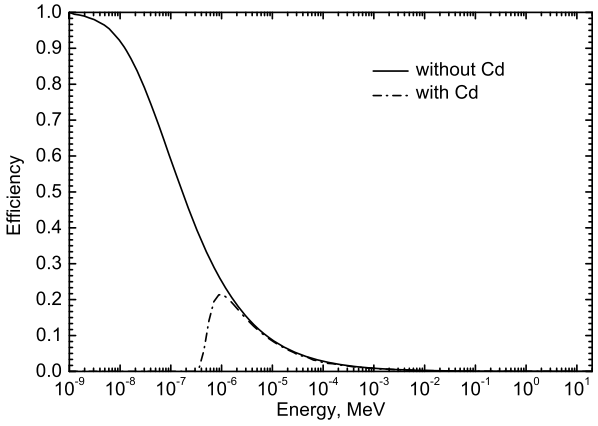

Fig. 6 The efficiency curves of DAN/DE CEN (*dashed line*) and DAN/DE CTEN (*solid line*) detectors. The low energy cut-off of CEN is produced by the Cd enclosure

time intervals between the moment of the start of neutron pulse and the moment of neutron detection. All counts detected in the instrument pulsing mode are distributed into 64 successive logarithmic time bins synchronized with the beginning of the neutron pulse. Sensors CEN and CTEN have high efficiency for the registration of thermal and significant efficiency for the registration of low energy epithermal neutrons (Fig. 6). One may suggest the following rough estimation of a number of detected counts from each pulse of PNG with 10^7 14 MeV neutrons. The PNG is ~1 meter above the surface, and the total irradiated spot with

a radius of ∼1 meter has the area about 3 m^2. The average number of injected neutrons per cm^2 of this spot is ∼50 particles per cm^2. About half of these neutrons would be lost in the subsurface, and another half (∼25 neutrons per cm^2) would leak out. The fraction of thermal particles with energy <0.4 eV in the leakage spectrum is about 3 % (taken from numerical simulations). For radiating a spot with the area of 3 m^2, one may ignore the geometrical dilution of the flux of neutrons for the sensor height ∼1 m above the surface. So, the sensor of thermal and epithermal neutrons CTEN with an efficient cross section ∼15 cm^2 would measure $n_{CTEN} \sim 10$ counts for each pulse.

Assuming that a typical measurement with pulsing the DAN/PNG will have duration $t_{op} = 100$ seconds, pulsing frequency $f_{PNG} = 10$ Hz and n_{CTEN} counts per pulse equal to 10, one would expect an accumulation of 10^4 counts in the CTEN sensor. For other measurements with different parameters $n_{CTEN}, t_{op}, f_{PNG}$ it may be scaled as

$$N \sim 10^4 (n_{CTEN}/10) \cdot (t_{op}/100\ \mathrm{s}) \cdot (f_{PNG}/10\ \mathrm{Hz})\ \mathrm{counts} \tag{2}$$

Assuming the frequency of pulsing $f_{PNG} = 10$ Hz, one gets an estimate for the average count rate of CTEN for thermal neutrons produced by PNG as $\langle F_{PNG} \rangle = n_{CTEN} \cdot f_{PNG} \sim 10^2\ \mathrm{cts\,s^{-1}}$. For the total area of CTEN about 20 cm^2, it is comparable with a count rate $F_{GCR} \sim 10^2\ \mathrm{cts\,s^{-1}}$ of stationary neutron albedo due to bombardment by GCRs (see for example Masarik and Reedy 1996). The counting rate in DAN sensors from neutrons from MMRTG was directly measured in ground operations before the launch. It is about 25 and 10 counts/sec for CTEN and CEN, respectively. In the DAN commissioning operations in the passive mode during the cruise stage, the total counting rate was measured as 35 counts/sec and 15 counts/sec for CTEN and CEN, respectively. The additional counts in space are produced by the mass of MSL spacecraft under the bombardment of GCR. On Mars the GCR component of this background will be larger by several times because the solid angle of emitting Martian surface is several times larger than one of the spacecraft. Therefore, one may assume that backgrounds from MMRTG and GCR have comparable count rate, $F_{MMRTG} < 10^2\ \mathrm{cts\,s^{-1}}$ at the DAN location. So, the average count rate from pulsing PNG is comparable with the background from GCR and MMRTG.

However, the time resolution of DE for the measurements of die-away time profiles allows detection of a much larger ratio between the count rate of neutrons from irradiation by PNG in comparison with the stationary count rate from GCRs and MMRTG. Indeed, estimating the count rate for the duration of the dynamic die-away emission t_{DAE} about 10 milliseconds, one obtains the count rate $F_{PNG} \sim 10^3\ \mathrm{cts\,s^{-1}}$. So, during this time, the count rate of the albedo neutrons produced by DAN/PNG is about 10 times larger than the count rate from neutrons produced by GCRs and MMRTG. The advantage of DAN/PNG is the possibility to measure the full time profile of the dynamic albedo of neutrons within 10–30 milliseconds after a pulse, and than to measure separately the stable neutron background during the time intervals of about 70–90 milliseconds before the next pulse.

3.4 Active and Passive Modes of DAN Operations

DAN has two modes of operations. DAN/PNG is pulsing in the *active mode*. The sensor CTEN measures die-away time profiles for the sum of thermal and epithermal neutrons. The sensor CEN measures die-away time profiles of epithermal neutrons above the Cd threshold at 0.4 eV. The examples of these two time profiles (numerically simulated for DAN detectors for the soil with average water content about 3 %) are presented in Fig. 7. To measure the time profile of the die-away of thermal neutrons below the Cd threshold, we subtract the profile of CEN from the profile of CTEN (Fig. 7). Data from DAN in the active mode

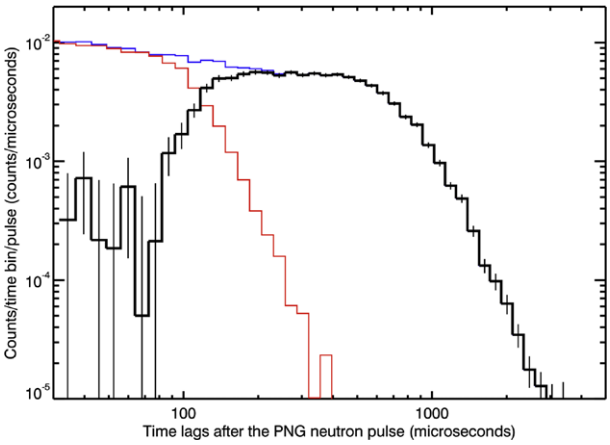

Fig. 7 The simulated die-away curves for DAN/DE CEN (*red curve*), and DAN/DE CTEN (*blue color*) are shown. The difference between counting rate of CTEN and CEN (*black solid line with uncertainties*) corresponds to the profile of thermal neutrons. The presented uncertainties correspond to the statistical significance of the simulated data

contains counts spectra in 16 channels, measured individually for each of 64 intervals of time lags during the total time of active mode operation. The logarithmic time scale can be set up into different configurations (the minimum duration of time bin can be changed in range 2–10 microseconds; maximum duration of time bin varies between 50–90 milliseconds). To adjust to the best conditions for measurements of thermal and epithermal neutrons from the Martian surface, one may change the low amplitude discriminator individually for each sensor and for the high voltages.

MSL has a minor fraction of hydrogen in the total mass, and high energy neutrons from DAN/PNG may backscatter by the mass of MSL. One may expect just a few scatterings of neutrons, which would take place during a time of 1–10 microseconds. Counts of backscattered neutrons should be similar at CTEN and CEN. So, using the time lag intervals longer then 10 microseconds, and also subtracting counts of CEN from counts of CTEN, one would get the albedo profiles for thermal neutrons from the Martian surface, which should not contribute neutrons scattered by MSL.

The mass of MSL will also scatter thermal and epithermal neutrons of die-away emission from the surface, which will be measured in addition to the counts from the direct neutron flux from the surface. It is rather difficult to evaluate the contribution of this backscattering effect, and it will be studied in future numerical simulations. However, the contribution of backscattering into the amplitude of the die-away time profile is rather small in comparison with the main effect from the direct albedo of neutrons, because the total number of scattering nuclei of MSL is much smaller than the number of last-scattering nuclei of the subsurface. Moreover, the backscattering effect does not change the relative variation of die-away profiles of thermal neutrons from one spot of measurements to another. Therefore, this effect will not influence the accomplishment of the main task of the DAN investigations: search for variations of the surface composition along the rover path and determination of the spots with the highest content of hydrogen in the soil. But for estimation of the absolute values of hydrogen content during the surface operations, the contribution of backscattering effect will be taken into account.

In the *passive mode*, DAN/PNG does not operate. In this mode CTEN and CEN measure the static neutron albedo of the Martian surface due to GCRs and the MMRTG. Data products for this mode include the spectra of counts gathered for a fixed exposure time, which may be changed by spacecraft commands (default value is 20 sec). While the active mode will be used at MSL stops only, the passive mode will be available during the rover motion.

The optimal choice between DAN operations in the passive and active modes will be part of the instrument strategy of operations, which has to be evaluated to get the best science output from the DAN investigation.

Tables 1 and 2 present the main instrument parameters. The power consumption of DAN is different for different modes of operations because pulsing DAN/PNG needs electrical power, which is proportional to the pulsing frequency. The time duration of the pulsing measurement, as well as frequency of pulsation, is varied by instrument commands. Therefore, one may get the same statistics of counts in DAN detectors with different pulsing frequencies and correspondingly with different power consumption.

4 Calibrations, Field Tests and Numerical Modeling of DAN Investigations

4.1 Calibrations and Field Tests of DAN

Two experimental programs of physical calibrations of DAN have been performed in the facilities of Dubna Joint Institute of Nuclear Researches. In the first program, the physical sensitivity of DAN sensors CEN and CTEN were measured using a reference source of neutrons. Measurements were performed with a calibrated ^{232}Cf neutron source encapsulated inside polyethylene spheres with different radii of 7.6 cm and 12.7 cm. Such sources provide a continuous neutron spectrum that is quite similar to the Martian leakage spectrum. Different distances and different angles were selected for these measurements to estimate and exclude the local background effects from the calibration data. These calibration measurements are necessary to estimate detector efficiencies and convert the counts in the sensors into the physical flux of neutrons.

Also, typical data with die-away time profiles have been obtained with pulsing DAN/PNG to measure the number of counts per pulse in the same configuration (distance between DAN/DE and DAN/PNG and height above surface) as onboard the MSL rover. The surface was composed of large blocks of concrete (a sample of the concrete was sent to the laboratory to get the elemental composition) with a rather small water content of $\sim$3 %, measured independently by heating a concrete sample. The total thickness of the "soil" model under DAN was about 5 meters and its surface area ($>$20 m^2) was much larger than the DAN footprint. The calibration facility building has very large sizes (surface area is about 60 m $\times$ 20 m and height is about 15 m), so the backscattering from surrounding mass (walls and roof) was quite small. The number of counts from the thermal die away emission was found to be about 10 counts (as expected from the numerical simulations). The preliminary results of the DAN calibrations were partially presented at several science conferences (Litvak et al. 2010, 2011) and now the detailed report of these calibrations is under the preparation to be submitted together with the DAN data to PDS data system and to be published in a refereed journal.

The second program was focused on the measurements of DAN capabilities to detect a local "water rich" spot with different distributions of water equivalent material, including cases where such a material was buried under the surface. In our tests we used polyethylene plates with horizontal sizes of 40 $\times$ 60 cm and with a thickness of 8 cm as a substitution for a local water layer. The polyethylene was buried at different depths inside a pit made in the concrete model of soil (to simulate water rich layer at depth) and covered above by silicon bricks (as a simulation of top relative dry layer with $\sim$3 % of water). The rover mockup with installed DAN, a special mechanical fixture to support DAN at the same position as onboard MSL, was placed right above the "water rich" spot. Results of five measurements

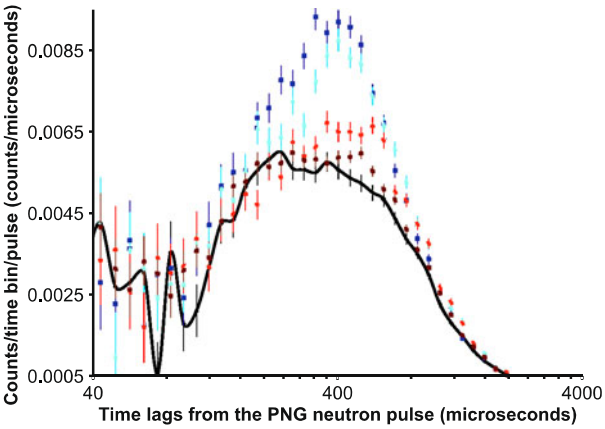

Fig. 8 The die-away curves of thermal neutrons measured by DAN/DE are presented for the different position of polyethylene layer in the hydrogen poor material (concrete). The *black curve* corresponds to the measurement (1) with no hydrogen spot in the subsurface (only H-poor subsurface with ∼3 % of water equivalent). The *blue curve* corresponds to the measurement (2) with the hydrogen rich material on the top of surface. The *cyan curve* corresponds to the measurement (3) with the hydrogen rich material at the depth ∼8 cm. The *red curve* corresponds to the measurement (4) with the hydrogen-rich material at the depth of ∼16 cm. The *brown curve* corresponds to the measurement (5) with the hydrogen rich material at the depth of ∼40 cm

are presented in Fig. 8: (1) no hydrogen spot (only H-poor subsurface with ∼3 % of water equivalent); (2) polyethylene on the top of surface; (3) polyethylene at the depth of ∼8 cm; (4) polyethylene at the depth of ∼16 cm; (5) polyethylene at the depth of ∼40 cm. One might see that time profiles of the thermal neutrons albedo in double layered cases (2)–(4) are obviously different from the hydrogen poor case (1). They are also different if we compare the limiting case (5) with the highest (40 cm) depth and case (1) with hydrogen poor material. Of course, on Mars our ability to see such a small effect as a difference between cases (5) and (1) has to be supported by large enough counting statistics to get the proper confidence of the observed difference and also verified by numerical modeling of neutrons albedo (see below).

As part of the second test program, the DAN flight model has also been tested in the *Polygon Field* of the Geological Faculty of Moscow State University (Zvenigorod, Moscow region, see for example Korolev et al. 2000). The field area occupies the bank of the Moscow river and consists of a bare homogeneous fluvioglacial sandy unit dated to be of late quaternary period according to a geological time scale. Several soil targets have been created for DAN tests at this field area. The main material of the targets was the quartz sand (main component of the soil) with different amount of absorbed water. Each target was 1-m in diameter, which roughly corresponds to the DAN neutron irradiation area. DAN was installed above the target on the special mechanical fixture in a position similar to the accommodation onboard MSL rover. The first target was the natural undisturbed soil. For other targets the upper layer (depth ranged 15–40 cm) of sand was removed, different amounts of water were added at the bottom and then the sand material was returned back to cover the created absorbed water lens. Following this procedure we have created several artificial double layered models of sand with relatively dry material on the top and wet bulk of the sand at the bottom at various depth 15–40 cm. The stability of such artificial targets was a few hours. During this period the active measurements with DAN were performed, and right afterward the bulk composition and structure of the target was independently analyzed by a geologist

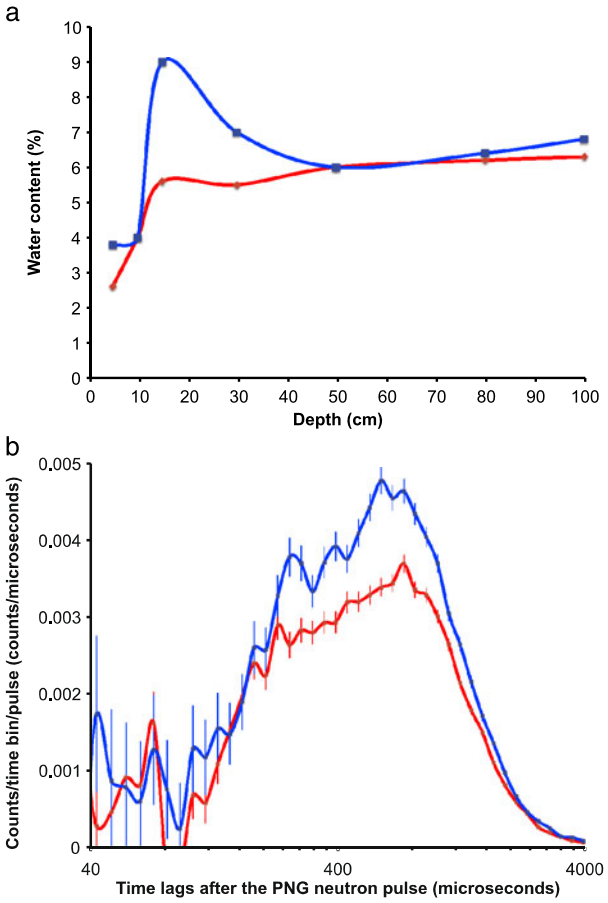

Fig. 9 (**a**) The water depth distribution for the two DAN field test targets of sand with different in-depth content of water. The water depth distribution for water-poor target is shown by *red color* and *blue color* is used to show water-rich target. (**b**) The die-away curves of thermal neutrons measured by DAN/DE in the field tests for water-rich target (*blue color*, see Fig. 9a for the water description) and for water-poor target (*red color*, see the Fig. 9a for the water description)

to derive estimations of various parameters as a function of depth, including absorbed water, density, structure of the soil and porosity. This analysis was done through the sampling of multiple probes of soil at different depths starting at 5 cm and down to 1 m. The resulting sand moisture varied within 2–9 wt% of water and was inhomogeneous with depth. Figure 9a illustrates two particular cases of targets with different water depth distributions. The first target presents natural undisturbed soil and the other one is the artificial double layered target with the maximum of absorbed water at the depth of 15 cm. Figure 9b shows the results of DAN measurements for these two particular targets. DAN measurements are presented as the die-away time profiles of thermal neutrons. It is seen that DAN should be able to distinguish these two targets with sufficient statistical significance.

So, the DAN physical calibrations and field tests are showing that the instrument is capable of distinguishing spots of the hydrogen rich material with different water content at different depths beneath the surface. Now we have started the program of numerical simulation of the DAN instrument using the library of various types of the Martian soil to get a quantitative estimation of DAN's sensitivity to water abundance in the Martian regolith. These simulation results will be compared with the data from past tests accomplished with DAN flight unit and with data from future field tests, which are now being planned with the DAN spare flight unit.

4.2 Numerical Simulations of DAN Measurements

The code of MCNPX (Pelowitz et al. 2005) has been used for comprehensive numerical simulations of DAN measurements. The content of the soil was selected to correspond with the average regolith composition measured by Mars Pathfinder mission (Wanke et al. 2001). The number of neutrons for Monte Carlo simulation was set up to 10^{10} to get high statistics during the simulation runs at the conditions of very long computational time required. During MSL surface operations the duration of DAN active measurements will be significantly (by an order of magnitude) varied depending on the rover resources available for the particular Martian sol. The measured differences in counting rates from one place to another will depend on the strength of the hydrogen variations along the rover's path. Strong variations of hydrogen abundance (for example from 1 % up to 10 % of water equivalent) will induce very significant changes (by 10 times) of the counting rate and will be easily detected for rather small measurement times, while very small hydrogen variations (<0.1 % of water equivalent) could not be detected even for very large measurement times. DAN will perform measurements with different statistics of counts but we expect that our simulation runs will correspond to the most frequent types of DAN measurements. These simulations help us to plan the duration of the measurements to be made by DAN depending on the magnitude of the effect.

DAN time profiles of data for thermal neutrons were calculated for different content and location of hydrogen in the soil. It was confirmed that the total number of detected counts of thermal neutrons measured per pulse is about 10 (for soils with a typical content of water of about 3 %). There are several options for the parameterization of DAN data for physical interpretations of die-away time profiles, (see for example Busch and Aharonson 2009; Hardgrove et al. 2011) and there are some approaches under development now to support DAN surface operations. Here we will use the technique described below.

The models of the soil have been studied numerically for variable content of hydrogen in the soil. The die-away profiles of thermal neutrons are different for different models: they have different amplitudes and different average time lags with respect to the start of a neutron pulse. It is convenient to characterize these profiles by two distinct parameters: by the total fluence C_{th} of counts of thermal neutrons, as the total sum of counts over the die-away profile, and by the average time-lag T_{th} of the die-away profile of thermal neutrons, as the average time-lag of all measured counts for these neutrons. The pairs of these parameters have been estimated for various simulated die-away profiles of thermal neutrons to derive useful quantitative signatures for comparing different cases of hydrogen depth distribution in Martian soil. One may expect that they will be used for a fast data analysis during Mars surface operations to detect the most promising areas with enhancement of hydrogen.

Figure 10 presents the results of simulations of the die-away emission of thermal neutrons for the soil with different distributions of hydrogen. These simulated data shown as a scatter plot of parameters (C_{th}, T_{th}). The orange curve represents the baseline case of homogeneous soil, with a content of hydrogen ξ that varies between 0–30 wt% of water equivalent. The total fluence of thermal neutrons C_{th} is increasing with increasing value of ξ. This result is consistent with the expectation from the physical concept of DAN (see Sect. 2) claiming that higher content of hydrogen means more neutrons reach the thermal equilibrium with the soil before leakage from the subsurface. The value of parameter C_{th} is increasing by ~6 times for ξ increasing from 1 % up to 30 wt%. It also indicates this parameter is quite sensitive to the variations of hydrogen content in the soil.

This orange curve has the minimum of time-lag T_{th} at ~380 microseconds, when $\xi \sim 2$ wt%. At the *low-hydrogen* case $\xi < 2$ wt%, the time-lag T_{th} is decreasing from

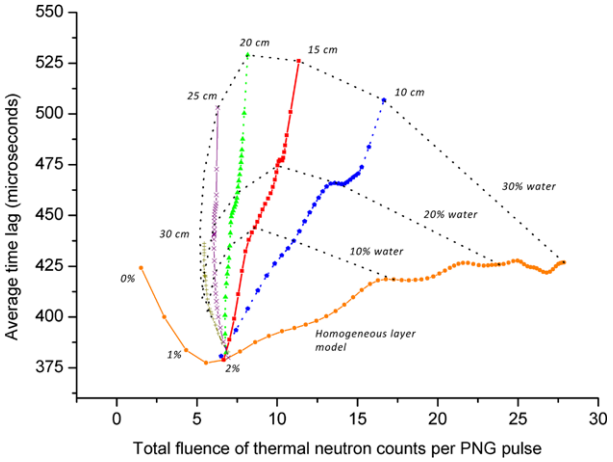

Fig. 10 The parameterization matrix of numerically simulated DAN measurements for homogeneous and two-layered models of Martian subsurface. The X-axis corresponds to the variations of total fluence of thermal neutron counts (per neutron pulse). The Y-axis corresponds to the average time lag of thermal neutrons emission relatively to the initial neutron pulses. The *orange color* is used to show the variation of DAN measurements for the homogeneous model of the regolith with different water content. The other colors correspond to measurable parameters the double layered models with different thickness of the top layer. The *dotted lines* shows variations of thermal emission parameters for changing depth of hydrogen-rich layer with the same content of water

425 microseconds at $\xi = 0$ % down to 380 microseconds at $\xi \sim 2$ wt%. One may explain this effect as the following: when a soil gets more hydrogen, the efficiency of thermalization is increasing, and more neutrons with small time-lags are thermalized before they leak from the surface. At the *high hydrogen* case $\xi > 2$ wt%, we observe the inverse tendency: the time-lag T_{th} is increasing up to the value of ~420 microseconds with increasing content of hydrogen. We understand that another physical effect of neutron diffusion dominates in this case: total time of random walk of neutrons before leaking is becoming longer for higher content of hydrogen, because more neutrons diffuse with thermal velocity between collisions. When the content of hydrogen becomes very high, corresponding to $\xi \sim 20$–30 wt% of water, the time-lag stays about the same ~420 microseconds with increasing content of hydrogen. In this case the time of thermalization of injected neutrons t_{th} is much smaller then the time t_{leak} of diffusive random walks needed to escape from the subsurface (see Sect. 2.2). Therefore, the dominant part of the thermal neutrons has been thermalized at the beginning of the diffusive leakage, and they are randomly walking with the thermal velocity V_{th}. The average time of a single walk is $\sim l_{fp}/V_{th}$, and the average time for leakage $t_{leak} = N_{leak} l_{fp}/V_{th}$ is not increasing with increasing content of hydrogen. So, estimating the pair of parameters (C_{th}, T_{th}) for the DAN die-away profiles of thermal neutrons, one may easily monitor the homogeneous soil with different content of hydrogen.

The different cases of two-layered models are also presented in Fig. 10. They present the simplest model with two distinct layers. The top layer is hydrogen-poor (in our analysis it was set to 2 wt% of water) with variable thickness from 0 to 30 cm. The underlying layer has the infinite thickness and variable content of hydrogen, corresponded to $\xi = 2$–30 wt% of water. The dashed lines in the Fig. 10 connect points of parameters (C_{th}, T_{th}), which corresponds to the same content of water in the underlying layer. It is evident (see Fig. 10) that cases of double layered models are qualitatively different from the cases of the homogeneous depth models. The average time lag T_{th} of thermal neutrons is systematically larger for the

double layered model. Neutrons thermalized in the hydrogen rich underlying layer have to complete additional random walks in the top layer before leakage. On the other hand, the average fluence C_{th} of thermal neutrons is systematically smaller for double layered model, because neutrons, which were thermalized in the underlying layer, could be backscattered and absorbed in the top layer.

The numerical simulation allows one to predict the observed behavior of parameters (C_{th}, T_{th}) for conditions when MSL with DAN will move to an area with a double layered structure of the soil, where the underlying layer has a variable content of hydrogen, and the top layer has a variable thickness. On Fig. 10 we have shown several trends of variations of (C_{th}, T_{th}) for the double layered models with 10, 20 and 30 wt% of water equivalent at depths 10, 15, 20, 25 and 30 cm. It illustrates that one would be able to use such an approach for fast data analysis to detect the most interesting spots with the highest content of hydrogen under the minimal layer of hydrogen-poor material.

5 Strategy of DAN Investigation

There are three types of DAN measurements on the Mars surface, that will be accomplished during the MSL mission:

- Active surface monitoring (ASM)
- Active surface analysis (ASA)
- Passive surface monitoring (PSM)

The measurements of active surface monitoring (ASM) and active surface analysis (ASA) are supported by active mode of DAN with pulsing PNG. In accordance with MSL surface operation rules, DAN may be switched onto the active mode with generation of neutron pulses only at MSL rover's stops (neutron pulsing during rover motion is prohibited). On the other hand the passive surface monitoring (PSM) may be performed continuously without any restrictions, but it can be interrupted during data passes to the Mars Reconnaissance or Mars Odyssey orbiters. We plan that DAN will provide PSM during all time periods, when the active mode of operations will not be possible.

DAN/PNG may emit a limited number of pulses, which are ensured by the instrument flight certification (10^7 pulses). Ground tests have shown that DAN/PNG may produce more neutron pulses than certified ones but its performance is not ensured in this case. The finite lifetime significantly influences the development of our strategy of DAN surface investigations. The main requirement is to find the optimal distribution for a limited number of neutron pulses between active surface monitoring (ASM) and active surface analysis (ASA) during the whole MSL mission. There are two unknowns for this development: one does not know (a) how many locations of HCAS with different composition could be found in the future for detailed analysis, and (b) what is the actual duration of the mission (e.g., life time of Mars Exploration Rovers was much larger than initial requirements).

The durations of one measurement of ASM and ASA are planned to be $\sim 10^2$ s and $\sim 10^4$ s, providing total statistics of counts $\sim 10^4$ and $\sim 10^6$ for measurements of die-away time profiles of thermal neutron neutrons for ASM and ASA, respectively (see Eq. (2)). It is planned that DAN/PNG will operate with the default frequency of 10 Hz, which leads to the generation of $\sim 10^3$ and $\sim 10^5$ pulses for ASM and ASA, respectively. We will use both types of measurements during the mission with equal distribution of pulsing resource between them. So, the full resource of pulsing of PNG allows $\sim 5 \cdot 10^3$ individual measurements for ASM and ~ 50 individual measurements for ASA. We expect that data from ASM will

allow measurement variations of the bulk hydrogen content in the subsurface with accuracy of 1 wt% of water equivalent for ASM and 0.1–0.2 % for ASA. The data from the ASM will also allow detection the strong signature of depth variations, such as illustrated in Figs. 9 and 10. The data from ASA will have much better statistics of counts for determination of the shape of die-away profiles, so these data will be mainly used to resolve depth distribution of hydrogen in HCAS regions selected for the detailed investigations.

We plan that ASM should be performed regularly during stops as MSL moves along the path in the Gale crater. Assuming the total distance of the path is ∼30 km, one may estimate that the average distance between spots of ASM measurements will be ∼6 meters. This discontinuity is appropriate to measure a continuous profile of variations of dynamic albedo of neutrons along the MSL path. In some interesting areas the measurements for ASM could be done with shorter distance between them, i.e. about 2–3 meters, but it is necessary to remember that it should be compensated by longer distances between successive measurements at other places (conserve keep pulsing resources for the whole mission). A region may be partially covered by PSM when a strong feature of hydrogen variation between two spots of ASM measurements could be resolved from passive monitoring, as an option of detailed investigation. We currently plan, that measurements of ASM at stops with measurements of PSM during the motion will be the baseline scenario for the initial stage of DAN investigations during 30–60 days.

The most challenging question is the selection of particular regions of interest for detailed analysis of hydrogen distribution, when the measurements of ASA type will be performed. Indeed, there are only ∼50 such individual measurements available, and each of them consumes 1 % of PNG pulsing capability. We believe that the best strategy of measurements of ASA will be developed during the initial stage of 30–60 days of the mission based on the first experience of surface operations. Currently, the algorithm for detection and study of one particular region of interest is suggested, as the following (Fig. 11):

- Using the data of ASM and PSM along the path of MSL, the distance profile of hydrogen variation is measured. If a local increase of hydrogen is found along the path, its limits and central point of local maximum should be identified (central point corresponds to the maximum of hydrogen content, or minimal depth of a hydrogen rich material).
- MSL performs the special circular maneuvers for localization of the potential region of interest with measurements of ASM and PSM (probably, with shorter distance of 2–3 meters between individual spots of ASM). The first circular maneuver #1 could be performed around the central point with crossing the limits. Using the data from the circle #1, one has to prove that the initial point of the maximal signal lies inside the contour of the circle #1. If it is not the case, the circular maneuver #2 is performed around the expected point of possible maximum of hydrogen, etc. Finally, the point of maximum should be localized inside some circle #N together with the line of maxima of hydrogen along the region of interest.
- N measurements of ASA could be performed inside the circles #1–#N at their central points. These data would characterize depth distribution of hydrogen/water along the line of maxima in the detected HCAS region (see Fig. 11).

We believe that this algorithm could be appropriate to study particular regions of interest with localization of maxima of the hydrogen distribution. It requires about 5 ASA measurements for one region, if this area is inspected by 5 circular maneuvers. The total number of studies regions would be 10 for the half of total pulsing resources of DAN. After obtaining some practical experience, one may revise the algorithm for a more efficient one, but in any case the total number of studied regions with ASA data could not be more than about 10–20 for the entire mission of MSL.

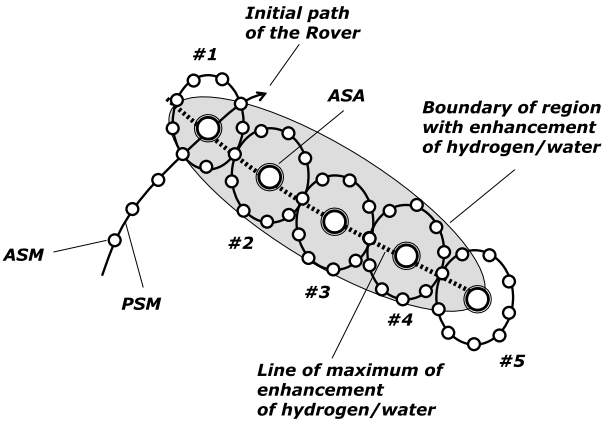

Fig. 11 Possible algorithm of detection and study of the HCAS region with enhancement of hydrogen/water

6 Conclusions

The measurements by DAN are consistent with the main goals of the MSL mission. When the rover will traverse along the Gale area from one particular region of detailed investigations to another one, DAN will mainly produce the data for the hydrogen distribution profile along the rover path. These measurements will characterize the soil composition in depth of about 0.5–1 meter. DAN data from monitoring measurements ASM and PSM will be available for joint analysis with data from other instruments onboard rover, which will allow understanding the nature of Gale surface along the traverse.

Some particular regions of interest could be detected from the monitoring data of DAN, or could be suggested from the data of other instruments. DAN has enough capabilities to study 10–20 regions of interest with ASA data for the analysis of depth distribution of hydrogen/water in the subsurface. Such data could be useful for selection of the best region with the largest content of hydrogen/water for excavation of subsurface material by rover wheels. The exact estimation of the depth to hydrogen bearing soil derived from the DAN data will be very important engineering parameter for performing such surface operations.

Acknowledgements In conclusion, the all DAN team would like to express their gratitude to the entire team of the MSL project for excellent professional support of DAN development and integration onboard the rover Curiosity. The authors are also very much thankful to anonymous reviewers of this paper for helpful comments, questions and language corrections, which have improved the original paper very much.

We wish to thank the International Space Science Institute (ISSI, Bern, Switzerland) for the support of researches (included in the framework of international team "Nuclear Planetology" in 2007–2010) presented in this paper.

References

I. Adler, J.I. Trombka, *Geochemical Exploration of the Moon and the Planets* (Springer, New York, 1970)

H. Akkurt, J.L. Groves, J. Trombka, R. Starr, L. Evans, S. Floyd, R. Hoover, L. Lim, T. McClanahan, R. James, T. McCoy, J. Schweitzer, Pulsed neutron generator system for astrobiological and geochemical exploration of planetary bodies. Nucl. Instrum. Methods Phys. Res. **241**, 232–237 (2005)

J.R. Arnold, A.E. Metzger, E.C. Anderson, M.A. van Dilla, Gamma rays in space. J. Geophys. Res. **67**, 4878–4880 (1962)

W.V. Boynton, W.C. Feldman, S.W. Squyres, T.H. Prettyman, J. Brückner, L.G. Evans, R.C. Reedy, R. Starr, J.R. Arnold, D.M. Drake, P.A. Englert, A.E. Metzger, I.G. Mitrofanov, J.I. Trombka, C. d'Uston, H. Wanke, O. Gasnault, D.K. Hamara, D.M. Janes, R.L. Marsialis, S. Maurice, I. Mikheeva, G.J. Taylor, R. Tokar, C. Shinohara, Distribution of hydrogen in the near surface of Mars: evidence for subsurface ice deposits. Science **297**, 81–85 (2002)

W.V. Boynton, W.C. Feldman, I.G. Mitrofanov, L.G. Evans, R.C. Reedy, S.W. Squyres, R. Starr, J.I. Trombka, C. d'Uston, J.R. Arnold, P.A.J. Englert, A.E. Metzger, H. Wanke, J. Bruckner, D.M. Drake, C. Shinohara, C. Fellows, D.K. Hamara, K. Harshman, K. Kerry, C. Turner, M. Ward, H. Barthe, K.R. Fuller, S.A. Storms, G.W. Thornton, J.L. Longmire, M.L. Litvak, A.K. Ton'chev, The Mars Odyssey gamma-ray spectrometer instrument suite. Space Sci. Rev. **110**, 37–83 (2004)

M.W. Busch, O. Aharonson, Measuring subsurface water distribution using the dynamic albedo of neutrons instrument on Mars science laboratory. Nucl. Instrum. Methods Phys. Res. **592**, 393–399 (2009)

D. De Soete, R. Gijbels, J. Hoste, *Neutron Activation Analysis* (Wiley, New York, 1972). ISBN-10 0471203904

B. Diez et al., Contribution of Mars Odyssey GRS at Central Elysium planitia. Icarus **200**, 19–29 (2009)

D.M. Drake, W.C. Feldman, B.M. Jakosky, Martian neutron leakage spectra. J. Geophys. Res. **93**, 6353–6368 (1988)

d'Uston, J.-L. Attea, C. Barat, A. Chernenko, V. Dolidze, A. Dyatchkov, E. Jourdain, V. Khariukova, N. Khavenson, A. Kozlenkov, R. Kucherova, I. Mitrofanov, M. Niel, A. Pozanenkio, P. Scheglov, Yu. Surkov, A. Vilchinskaya, Observations of the gamma-ray emission from the martian surface by the APEX experiment. Nature **431**, 598–600 (1989)

D.V. Ellis, J.M. Singer, *Well Logging for Earth Scientists, Pulsed Neutron Spectroscopy* (Springer, Berlin, 2007), pp. 383–414. doi:10.1007/978-1-4020-4602-5_15

L.G. Evans, R.D. Starr, J. Bruckner, R.C. Reedy, W.V. Boynton, J.I. Trombka, J.O. Goldsten, J. Masarik, L.R. Nittler, T.J. McCoy, Elemental composition from gamma-ray spectroscopy of the NEAR-Shoemaker spacecraft's landing site on Eros. Meteorit. Planet. Sci. **36**, 1639–1660 (2001)

W.C. Feldman, S. Maurice, D.J. Lawrence, R.C. Little, S.L. Lawson, O. Gasnault, R.C. Wiens, B.L. Barraclough, R.C. Elphic, T.H. Prettyman, J.T. Steinberg, A.B. Binder, Evidence for water ice near the lunar poles. J. Geophys. Res. **106**(E10), 23231–23252 (2001)

W.C. Feldman, W.V. Boynton, R.L. Tokar, T.H. Prettyman, O. Gasnault, S.W. Squyres, R.C. Elphic, D.J. Lawrence, S.L. Lawson, S. Maurice, G.W. McKinney, K.R. Moore, R.C. Reedy, Global distribution of neutrons from Mars: results from Mars Odyssey. Science **297**, 75–78 (2002)

W.C. Feldman, K. Ahola, B.L. Barraclough, R.D. Belian, R.K. Black, R.C. Elphic, D.T. Everett, K.R. Fuller, J. Kroesche, D.J. Lawrence, S.L. Lawson, J.L. Longmire, S. Maurice, M.C. Miller, T.H. Prettyman, S.A. Storms, G.W. Thornton, Gamma-ray, neutron, and alpha-particle spectrometers for the lunar prospector mission. J. Geophys. Res. **109**, E07S06 (2004a). doi:10.1029/2003JE002207

W.C. Feldman, T.H. Prettyman, S. Maurice, J.J. Plaut, D.L. Bish, D.T. Vaniman, M.T. Mellon, A.E. Metzger, S.W. Squyres, S. Karunatillake, W.V. Boynton, R.C. Elphic, H.O. Funsten, D.J. Lawrence, R.L. Tokar, Global distribution of near-surface hydrogen on Mars. J. Geophys. Res. **109**, E09006 (2004b). doi:10.1029/2003JE002160

J.O. Goldsten, E.A. Rhodes, W.V. Boynton, W.C. Feldman, D.J. Lawrence, J.I. Trombka, D.M. Smith, L.G. Evans, J. White, N.W. Madden, P.C. Berg, G.A. Murphy, R.S. Gurnee, K. Strohbehn, B.D. Williams, E.D. Schaefer, C.A. Monaco, C.P. Cork, J.D. Eckels, W.O. Miller, M.T. Burks, L.B. Hagler, S.J. DeTeresa, M.C. Witte, The MESSENGER gamma-ray and neutron spectrometer. Space Sci. Rev. **131**, 339–391 (2007)

J.P. Grotzinger, J. Crisp, A.R. Vasavada, R.C. Anderson, C.J. Baker, R. Barry, D.F. Blake, P. Conrad, K.S. Edgett, B. Ferdowski, R. Gellert, J.B. Gilbert, M. Golombek, J. Gómez-Elvira, D.M. Hassler, L. Jandura, M. Litvak, P. Mahaffy, J. Maki, M. Meyer, M.C. Malin, I. Mitrofanov, J.J. Simmonds, D. Vaniman, R.V. Welch, R.C. Wiens, Mars Science Laboratory Mission and science investigation. Space Sci. Rev. (2012). doi:10.1007/s11214-012-9892-2, this issue.

C. Hardgrove, J. Moersch, D. Drake, Effects of geochemical composition on neutron die-away measurements: implications for Mars science laboratory's dynamic albedo of neutrons experiment. Nucl. Instrum. Methods Phys. Res. A **659**(1), 442–455 (2011)

I. Jun, W. Kim, M. Smith, I. Mitrofanov, M. Litvak, A study of Venus surface elemental composition from 14 MeV neutron induced gamma ray spectroscopy: activation analysis. Nucl. Instrum Methods Phys. Res. A **629**(1), 140–144 (2011)

G.F. Knoll, *Radiation Detection and Measurements*, 3rd edn. (Wiley, New York, 2000), p. 554

V.A. Korolev et al., *Hydrogeology, Engineering Geology, Cryopedology and Ecological Geology Methods Applicable to the Field Tests* (Moscow State University Press, Moscow, 2000). ISBN 5-211-04114-3

D.J. Lawrence, W.C. Feldman, R.C. Elphic, R.C. Little, T.H. Prettyman, S. Maurice, P.G. Lucey, A.B. Binder, Iron abundances on the lunar surface as measured by the lunar prospector gamma-ray and neutron spectrometers. J. Geophys. Res. **107**(E12), 5130 (2002). doi:10.1029/2001JE001530

M.L. Litvak, I.G. Mitrofanov, A.S. Kozyrev, A.B. Sanin, V.I. Tretyakov, W.V. Boynton, N.J. Kelly, D. Hamara, C. Shinohara, R.S. Saunders, Comparison between polar regions of Mars from HEND/Odyssey data. Icarus **180**, 23–37 (2006)

M.L. Litvak, I.G. Mitrofanov, Yu.N. Barmakov, A. Behar, A. Bitulev, Yu. Bobrovnitsky, E.P. Bogolubov, W.V. Boynton, S.I. Bragin, S. Churin, A.S. Grebennikov, A. Konovalov, A.S. Kozyrev, I.G. Kurdumov, A. Krylov, Yu.P. Kuznetsov, A.V. Malakhov, M.I. Mokrousov, V.I. Ryzhkov, A.B. Sanin, V.N. Shvetsov, G.A. Smirnov, S. Sholeninov, G.N. Timoshenko, T.M. Tomilina, D.V. Tuvakin, V.I. Tretyakov, V.S. Troshin, V.N. Uvarov, A. Varenikov, A. Vostrukhin, The dynamic albedo of neutrons (DAN) experiment NASA's 2009 Mars science laboratory. Astrobiology **8**(3), 605–612 (2008)

M.L. Litvak, I.G. Mitrofanov, V.N. Shvecov, G.N. Timoshenko, A.S. Kozyrev, A.V. Malakhov, M.I. Mokrousov, A.B. Sanin, V.I. Tretyakov, A.A. Vostrukhin, DAN/MSL instrument: first field tests, in *41st Lunar and Planetary Science Conference, held March 1–5, 2010 in The Woodlands, Texas* (2010), p. 2021. LPI Contribution No. 1533

M.L. Litvak, I.G. Mitrofanov, V.N. Shvecov, G.N. Timoshenko, A.S. Kozyrev, A.V. Malakhov, M.I. Mokrousov, A.B. Sanin, V.I. Tretyakov, A.A. Vostrukhin, A.B. Varenikov, Studies of layering structure of Martian subsurface by active neutron experiment DAN onboard MSL, in *42nd Lunar and Planetary Science Conference, held March 7–11, 2011 at The Woodlands, Texas* (2011), p. 1776. LPI Contribution No. 1608

Masarik, Reedy, Gamma ray production and transport in Mars. J. Geophys. Res. **101**(E8) (1996). doi:10.2029/96JE01563

A.E. Metzger, J.I. Trombka, L.E. Peterson, R.C. Reedy, J.R. Arnold, Lunar surface radioactivity: preliminary results of the Apollo 15 and Apollo 16 gamma ray spectrometer experiments. Science **179**, 800–803 (1973)

I.G. Mitrofanov, D. Anfimov, A. Kozyrev, M. Litvak, A. Sanin, V. Tret'yakov, A. Krylov, V. Shvetsov, W.V. Boynton, C. Shinohara, D. Hamara, R.S. Saunders, Maps of subsurface hydrogen from the high energy neutron detector, Mars Odyssey. Science **297**, 78–81 (2002)

I.G. Mitrofanov, M.L. Litvak, A.S. Kozyrev, A.B. Sanin, V.I. Tret'yakov, W.V. Boynton, C. Shinohara, D. Hamara, R.S. Saunders, D. Drake, Search for water in Martian soil using global neutron mapping by the Russian HEND instrument onboard the US 2001 Mars Odyssey spacecraft. Sol. Syst. Res. **37**, 366–377 (2003)

I.G. Mitrofanov, M.L. Litvak, A.S. Kozyrev, A.B. Sanin, V.I. Tret'yakov, W.V. Boynton, C. Shinohara, D. Hamara, R.S. Saunders, Estimation of water content in Martian regolith from neutron measurements by HEND onboard 2001 Mars Odyssey. Sol. Syst. Res. **38**(4), 253–257 (2004)

I.G. Mitrofanov, A.B. Sanin, D.V. Golovin, M.L. Litvak, A. Konovalov, A.S. Kozyrev, A.V. Malakhov, M.I. Mokrousov, V.I. Tretyakov, V.S. Troshin, V.N. Uvarov, A.B. Varenikov, A.A. Vostrukhin, V.V. Shevchenko, V.N. Shvetsov, A.R. Krylov, G.N. Timoshenko, Y.I. Bobrovnitsky, T.M. Tomilina, A.S. Grebennikov, L.L. Kazakov, R.Z. Sagdeev, G.N. Milikh, A. Bartels, G. Chin, S. Floyd, J. Garvin, J. Keller, T. McClanahan, J. Trombka, W.V. Boynton, K. Harshman, R. Starr, L. Evans, Experiment LEND of the NASA lunar reconnaissance orbiter for high-resolution mapping of neutron emission of the Moon. Astrobiology **8**(4), 793–804 (2008)

I.G. Mitrofanov, A. Bartels, Y.I. Bobrovnitsky, W.V. Boynton, G. Chin, H. Enos, L. Evans, S. Floyd, J. Garvin, D.V. Golovin, A.S. Grebennikov, K. Harshman, L.L. Kazakov, J. Keller, A. Konovalov, A.S. Kozyrev, A.R. Krylov, M.L. Litvak, A.V. Malakhov, T. McClanahan, G. Milikh, M.I. Mokrousov, S. Ponomareva, R.Z. Sagdeev, A.B. Sanin, V.V. Shevchenko, V.N. Shvetsov, R. Starr, G.N. Timoshenko, T.M. Tomilina, V.I. Tretyakov, J. Trombka, V.S. Troshin, V.N. Uvarov, A. Varenikov, A.A. Vostrukhin, Lunar exploration neutron detector for the NASA lunar reconnaissance orbiter. Space Sci. Rev. **150**(1–4), 183–207 (2010a)

I.G. Mitrofanov, A.B. Sanin, W.V. Boynton, G. Chin, J.B. Garvin, D. Golovin, L.G. Evans, K. Harshman, A.S. Kozyrev, M.L. Litvak, A. Malakhov, E. Mazarico, T. McClanahan, G. Milikh, M. Mokrousov, G. Nandikotkur, G.A. Neumann, I. Nuzhdin, R. Sagdeev, V. Shevchenko, V. Shvetsov, D.E. Smith, R. Starr, V.I. Tretyakov, J. Trombka, D. Usikov, A. Varenikov, A. Vostrukhin, M.T. Zuber, Hydrogen mapping of the lunar south pole using the LRO neutron detector experiment LEND. Science **330**(6003), 483 (2010b)

A. Parsons, J. Bodnarik, L. Evans, S. Floyd, L. Lim, T. McClanahan, M. Namkung, S. Nowicki, J. Schweitzer, R. Starr, J. Trombka, Active neutron and gamma-ray instrumentation for in situ planetary science applications. Nucl. Instrum. Methods Phys. Res. A **652**(1), 674–679 (2011)

D.B. Pelowitz et al., MNCPX User's Manual, Version 2.5.0, LANL. Los Alamos (2005). LA-UR-05-0369

T.H. Prettyman, W.C. Feldman, M.T. Mellon, G.W. McKinney, W.V. Boynton, S. Karunatillake, D.J. Lawrence, S. Maurice, A.E. Metzger, J.R. Murphy, S. Squyres, R.D. Starr, R.L. Tokar, Composition and structure of the Martian surface at high southern latitudes from neutron spectroscopy. J. Geophys. Res. **109** (2004). doi:10.1029/2003JE002139

T.H. Prettyman, W.C. Feldman, H.Y. McSween, R.D. Dingler, D.C. Enemark, D.E. Patrick, S.A. Storms, J.S. Hendricks, J.P. Morgenthaler, K.M. Pitman, R.C. Reedy, Dawn's gamma ray and neutron detector. Space Sci. Rev. **163**(1–4), 371–459 (2011)

E.A. Rhodes, L.G. Evans, L.R. Nittler, R.D. Starr, A.L. Sprague, D.J. Lawrence, T.J. McCoy, K.R. Stockstill-Cahill, J.O. Goldsten, P.N. Peplowski, Analysis of MESSENGER gamma-ray spectrometer data from the Mercury flybys. Planet. Space Sci. **59**(15), 1829–1841 (2011)

M.A. Riner, P.G. Lucey, F.M. McCubbin, G.J. Taylor, Constraints on Mercury's surface composition from MESSENGER neutron spectrometer data. Earth Planet. Sci. Lett. **308**(1), 107–114 (2011)

Y.A. Surkov, F.F. Kirnozov, I.N. Ivanov, G.M. Kolesov, B.N. Ryvkin, A.P. Shpanov, Neutron-activation analysis of lunar soil brought back from Mare Fecunditatis by Luna-16. Cosm. Res. **11**, 860 (1973)

A.P. Vinogradov, Yu.A. Surkov, G.N. Chernov, F.F. Kirnozov, G.B. Nazarkina, Measurement of the gamma radiation of the lunar surface by the Luna-10 spacecraft. Cosm. Res. **4**, 751–755 (1966)

H. Wanke, J. Bruckner, G. Dreibus, R. Rieder, I. Ryabchikov, Chemical composition of rocks and soils at the Pathfinder site. Space Sci. Rev. **96**, 317–330 (2001)